Supporting Information

Bard et al. 10.1073/pnas.1002690107

SI Materials and Methods

Ligand Synthesis and in Vitro Characterization. The design and synthesis (M.S., B.I.) of peptide-based ligands is schematically described in this paragraph. Briefly, the last 15 residues of the ligand binding motifs were first assembled by standard Fmoc-based solid phase peptide synthesis and capped with a mixture of azide- and alkyne-derived acids. The ligation was conducted by click chemistry (1) on resin. For the 4-DMAP-containing ligand, the fluorophore was inserted post ligation on resin. The TAT sequence was coupled as a C-terminal thioester to the purified ligand N-terminal Cys residue by native chemical ligation. BODIPY-FL was coupled using a maleimide derivative to the same Cys residue. Recombinant PSD-95 tandem PDZ domains expression and fluorescence titrations were performed as previously described (2).

Single Particle (QD) Tracking and Surface Diffusion Calculation. QD 655 Goat F(ab′)2 anti-Rabbit or anti-mouse IgG (Invitrogen) were first incubated for 30 min with the polyclonal antibodies against NR2A (1 μg) and NR2B subunits (1 μg), the monoclonal anti-Flag (Stratagene), the anti $GABA_A$ α2 (gift from A. Triller, Ecole Normale Superieure, Paris), and the Kv1.3 antibodies (Alomone Labs; epitope location corresponds to the first extracellular loop between domains S1 and S2 amino acid, i.e., residues 263–276 of Kv1.3). For this Kv1.3 antibody, specificity control has been obtained only with Western blot (Alomone Labs). Nonspecific binding was blocked by additional casein (Vector Laboratories) to the QD 15 min before use. For experiments using TAT peptides, neurons were first incubated for 10 min at 37 °C in culture medium with precoated QDs (final dilution 1:2,000 for anti-NR2A and anti-NR2B coupled QDs, 1:10,000 for anti-$GABA_A$ coupled QDs, 1:5,000 for anti-kv1.3 coupled QDs), then for 1 min with 20 nM Green Mitotracker (Molecular Probes), for 5 min with 50 μM pyrene butyrate (3) and finally for 10 min with 5 μM TAT-$[NS_{15}]_2$ or TAT-$[NR2A_{15}]_2$ (or TAT-$NR2B_{15}$ when specified).

We first examined the penetration of the TAT-$[NR2A_{15}]_2$ in neurons. As shown in Fig. S10, the ligand efficiently penetrates cultured neurons and was observed in all dendritic compartments, including postsynaptic densities. We next tested the nonspecific effects of pyrene butyrate or TAT-$[NS_{15}]_2$ on the mobility of 2A-NMDARs (Fig. S11). Whereas pyrene butyrate had no effect per se, TAT-$[NS_{15}]_2$ increased the proportion of immobile receptors. Importantly, such effect of TAT-$[NS_{15}]_2$ was observed on 2B-NMDARs, GluR2-AMPARs, $GABA_A$Rs, and reproduced using the monomeric TAT-$[NS_{15}]$. This indicates that TAT-$[NS_{15}]_2$ slightly reduced the surface trafficking of neurotransmitter receptors, irrespective of the nature of the receptors or the structure of the TAT ligand.

For single particle tracking of Flag-tagged NR2B subunits, neurons were incubated for 10 min with precoated anti-Flag QDs (final dilution, 1:10,000). QDs were detected by using a mercury lamp and appropriate excitation/emission filters. Images were obtained with an integration time of 5 to 30 ms with up to 2,000 consecutive frames. Signals were detected using a CCD camera (Quantem; Roper Scientific). QDs were followed on randomly selected dendritic regions for up to 20 min. QD recording sessions were processed with Metamorph software (Universal Imaging). The instantaneous diffusion coefficient, D, was calculated for each trajectory, from linear fits of the first four points of the MSD versus time function:

$$\mathrm{MSD}(t) = \langle r^2 \rangle (t) = 4Dt \qquad \textbf{[S1]}$$

Synaptic dwell time was calculated for exchanging receptors and defined as the mean time spent within the synaptic area. The 2D trajectories of single molecules in the plane of focus were constructed by correlation analysis between consecutive images using a Vogel algorithm.

Cell Culture, Immunocytochemistry, Synaptic Live Staining, and Protein Expression. Cultures of hippocampal neurons were prepared from E18 Sprague–Dawley rats following a previously described method (4–6). Briefly, cells were plated at a density of 100 to 200×10^3 cells per milliliter on poly-lysine precoated coverslips. Cultures were maintained in serum-free neurobasal medium (Invitrogen) and kept at 37 °C in 5% CO_2 for 20 d in vitro at maximum. For immunostaining, surface 2A-NMDARs were specifically stained using a polyclonal anti-NR2A subunit antibody (1:100; F. A. Stephenson, London, United Kingdom) for 15 min on live neurons at 37 °C in culture medium. The specificity of the antibody was previously described (5). Briefly, neurons were then fixed with 4% paraformaldehyde/4% sucrose for 15 min, washed, and incubated with secondary antibodies anti-rabbit Alexa 488 antibodies (1:1,000, 45 min; Molecular Probes). To label postsynaptic areas, neurons were permeabilized using 0.1% Triton X-100, incubated with a primary rabbit polyclonal anti-shank antibody (1:750, 45 min; Abcam), and finally incubated with secondary antibody anti-rabbit Alexa 568 antibodies (1:1,500, 30 min; Molecular Probes). Neurons were washed and mounted and preparations were kept at 4 °C until quantification. For the quantification of surface NR2A staining within individual shank cluster, the shank-synaptic staining served as a mask filter to isolate surface NR2A staining in individual shank clusters. The integrated fluorescence level over the shank-cluster area was then measured for each cluster. The fluorescence analysis was realized using imaging tools from Metamorph software (Universal Imaging). To label synapses live cultured neurons were incubated for 1 to 2 min at room temperature with 10 nM Mitotracker (Deep Red-Fluorescent Mitotracker; Molecular Probes) prior to imaging experiments. Neurons were transfected at 7 to 10 d in vitro with Homer1c-DsRed or Homer1c-GFP alone or with SEP-NR1, SEP-NR2A, or SEP-NR2B using the Effectene transfection kit (Qiagen). We mixed 2 μg of DNA with 25 μL of Effectene and 8 μL of enhancer in 150 μL of reaction buffer, and then added the mixture to cultured neurons, which were transferred to serum-free neurobasal medium 10 min beforehand. After an incubation period of 45 min, neurons were placed in the old medium again.

Postsynaptic Localization of NMDARs. Surface diffusion of postsynaptic NMDARs has been described using electrophysiological and high-resolution imaging approaches (5, 7–9). It is noteworthy that the diffusion of presynaptic NMDARs has also been described in synapses from the entorhinal cortex at early stages of development (10). Because single particle tracking on endogenous NMDARs does not distinguish between pre- and postsynaptic receptors, we investigated whether presynaptic tagged NMDARs were present in our hippocampal system. However, we found no evidence for surface NMDARs in presynaptic (VAMP-2-positive cluster) terminals, indicating that in our neuronal preparation surface NMDARs are mostly located in the postsynaptic area.

Electrophysiology. Neurons were continuously perfused with extracellular solution containing (in mM): 145 NaCl, 2.5 KCl, 10 Hepes, 10 glucose, 2 $CaCl_2$, and 0.1 mM Mg^{2+}, pH 7.3, osmolarity 300

mOsm/L. Patch pipettes (3–5 MΩ) were filled with (in mM): 140 cesium methanesulfonate, 2 $MgCl_2$, 4 NaCl, 5 phosphocreatine, 10 Hepes, 2 Na_2-ATP, 0.33 Na-GTP, 5 QX-314, and 0.2 EGTA, pH 7.3, osmolarity 290 mOsm/L. Recordings in voltage clamp mode were performed with an EPC 10 double patch-clamp amplifier (HEKA). Recordings included for analysis were collected during periods of stable series resistance. Data were acquired and stored using Pulse-Pulse fit software, version 8.62. Miniature NMDAR EPSCs were recorded at +40 mV and isolated in the presence of TTX (1 μM), bicuculline (20 μM; Ascent Scientific), and NBQX (10 μM, Ascent Scientific). Miniature AMPAR EPSCs were recorded at −50 mV and isolated in the presence of TTX (1 μM), bicuculline (20 μM; Ascent Scientific), and AP5 (25 μM; Ascent Scientific) (11). Miniature EPSCs were analyzed by using the Mini-Analysis program (version 6.0.7; Synaptosoft) and IGOR (WaveMetrics). The limit of detection was greater than 5 pA. The decay times of NMDA-mEPSCs were fitted using two exponentials.

Hippocampal slices were prepared from P16-20 C57Bl6 mice. Mice were decapitated and the brain was removed and placed in ice-cold solution composed of (in mM): 87 NaCl, 2.5 KCl, 10 glucose, 75 sucrose, 25 $NaHCO_3$, 1.25 NaH_2PO_4, 0.5 $CaCl_2$, and 7 mM Mg^{2+}. Transverse hippocampal slices (350 μm) were cut using a vibrating tissue slicer (Leica) and transferred to a holding chamber and stored at 33 °C. For recording, slices were individually transferred to a recording chamber where they were perfused at 30 °C to 35 °C. The extracellular solution contained (in mM): 125 NaCl, 2.5 KCl, 25 glucose, 26 $NaHCO_3$, 1.25 NaH_2PO_4, 2 $CaCl_2$, and 1 mM Mg^2. $GABA_AR$ postsynaptic currents were blocked by 20 μM bicuculline. AMPAR EPSCs were blocked by 10 μM NBQX. CA1 pyramidal cells were visually identified using IR-DIC videomicroscopy and whole-cell patch-clamp recordings were performed with an EPC-10 patch-clamp amplifier (HEKA). The pipette solution contained (in mM): 140 cesium methanesulfonate, 2 $MgCl_2$, 4 NaCl, 5 phosphocreatine, 10 Hepes, 2 Na_2-ATP, 0.33 Na-GTP, 5 QX-314, and 0.2 EGTA, pH 7.3, osmolarity 290 mOsm/L. Patch pipettes were pulled using a horizontal puller (Sutter Instruments) and their resistance was 3 to 5 MΩ. The series resistance, which was continuously monitored during the experiments using a 5-mV hyperpolarizing pulse. Recordings included for analysis were collected during periods of stable series resistance. Recordings with series resistance greater than 20 MΩ were discarded. Responses were sampled at 10 kHz. A glass pipette filled with extracellular solution (NaCl 0.9%) was used to evoke unitary NMDA EPSCs. The pipette was placed in the stratum radiatum of the CA1 area. Stimulations were applied at 0.05 Hz and the cells were held at +30 mV.

FRAP and Follow-Up of Cluster Fluorescence Intensity. SEP-NR1 and Homer1c-DsRed cotransfected neurons were placed on the heated stage (37 °C) of an inverted confocal spinning-disk microscope (Leica). To test the population of surface SEP-NR1, we used low-pH solution adjusted to pH 5.4, which quenched all of the fluorescence indicating that SEP allows the specific visualization of surface receptors. Fluorescence was excited using a monochromator controlled by Metamorph software (Universal Imaging). To photobleach locally, we used a sapphire laser 488–20 to 50% power to avoid photo damage. The laser was coupled to the microscope via a galvometric mirror, which allowed us to photobleach several regions within a short time window. Recovery from photobleaching was monitored by two consecutive acquisition periods at 2 and 0.5 Hz acquisition rates, respectively. Recovery curves were corrected for continuous photobleaching and background noise. For the follow-up of cluster fluorescence intensity to assess receptor content, neurons were cotransfected with Homer1c-DsRed and either SEP-NR2A or SEP-NR2B. Clusters were imaged over a period of 20 min after acute addition of 5 μM TAT-$[NS_{15}]_2$ or TAT-$[NR2A_{15}]_2$. Fluorescence intensity was measured using Metamorph software (Universal Imaging) and corrected for photobleaching and background noise.

Immunoprecipitation and Western Blot Analysis. A frozen adult rat brain (approximately 1.6 g) was thawed in 16 mL ice cold SHC buffer (320 mM sucrose, 1 mM Hepes, 1 mM $MgCl_2$, 1 mM $NaHCO_3$) containing a protease inhibitor mixture (1:1,000; Calbiochem) for 5 min and cut into small pieces. The tissue was homogenized using a Teflon-glass homogenizer and the homogenate was spun at 1,000 × *g* for 10 min at 4 °C. The resulting supernatant was spun at 10,000 × *g* for 15 min to obtain a P2 crude membrane fraction. P2 pellets were divided into aliquots and stored at −80 °C until solubilization and immunoprecipitation reactions were performed.

P2 fractions were solubilized with RIA buffer containing 1% SDS (200 mM NaCl, 10 mM EDTA, 10 mM Na_2HPO_4, 0.5% Nonidet P-40, 1% SDS) for 5 min at 4 °C, followed by dilution to 0.1% SDS. The resulting lysate (200 μg of protein) was diluted in RIA buffer containing 0.1% SDS, followed by incubation under constant agitation at 37 °C for 15 min with ligand TAT-$[NR2A_{15}]_2$ (1.5 μM), TAT-$[NS_{15}]_2$ (1.5 μM), or a similar volume of dH_2O. NR2A (0.6 μg, AGC-002; Alomone Labs) or NR2B (0.8 μg, polyclonal antibody described in ref. 7) antibodies were incubated under constant agitation at 37 °C for 15 min with 10 μL of prewashed Protein A beads (Dynabeads Protein A; Invitrogen). The lysates were added to the antibody-bead mixtures and incubated under constant agitation overnight at 4 °C. Immunoprecipitates were separated by SDS/PAGE and analyzed by Western blotting using a rabbit monoclonal antibody to NR2A (04-901, clone A12W; Millipore), a rabbit polyclonal antibody to NR2B (A-6474; Molecular Probes), or a mouse monoclonal antibody to PSD-95 (MA1-046; Thermo Scientific). Detection was performed using the SuperSignal West Femto Maximum Sensitivity Substrate detection kit (Pierce), revealed with a Chemigenius system (Syngene). Quantification of bands intensity was performed using Genetools software (Syngene).

In Vitro Cell Surface Assay. HEK 293 cells were cotransfected in triplicate in 24-well tissue culture plates with either pCIS vector, NR1-1a/NR2A or NR1-1a/NR2B NMDA receptors in the presence and absence of PSD-95 (2 μg of total DNA per well). Post-transfection (24 h), cells were incubated with either vehicle control, TAT-$[NR2A_{15}]_2$ or control TAT-$[NS_{15}]_2$ (10 μM) for 1 h at 37 °C. Cell surface NMDA receptor expression was determined by ELISA with affinity-purified antibodies directed against extracellular epitopes of NR2A and NR2B, i.e., anti-NR2A 44–58 Cys (0.25 μg/mL) or anti-NR2B 46–60 Cys (0.5 μg/mL).

Data and Statistical Analysis. The instantaneous diffusion coefficient is reported as the median ± 25% to 75% (i.e., IQR). All of the other group values are expressed as mean ± SEM. Comparisons between groups for instantaneous diffusion coefficients were performed using Mann–Whitney test (pair comparison) or Kruskal-Wallis followed by Dunn multiple-comparison test (group comparison). All of the other comparisons between groups were performed using parametric statistical tests, Student *t* test (pair comparison), ANOVA followed by Newman–-Keuls multiple comparison test (group comparison), or Kolmogorov–Smirnov test (distribution comparison). Significance levels were defined as $P < 0.05$, $P < 0.01$, and $P < 0.001$.

1. Rostovtsev VV, Green LG, Fokin VV, Sharpless KB (2002) A stepwise Huisgen cycloaddition process: Copper(I)-catalyzed regioselective "ligation" of azides and terminal alkynes. *Angew Chem Int Ed Engl* 41:2596–2599.

2. Sainlos M, Iskenderian WS, Imperiali B (2009) A general screening strategy for peptide-based fluorogenic ligands: Probes for dynamic studies of PDZ domain-mediated interactions. *J Am Chem Soc* 131:6680–6682.

3. Takeuchi T, et al. (2006) Direct and rapid cytosolic delivery using cell-penetrating peptides mediated by pyrenebutyrate. *ACS Chem Biol* 1:299–303.
4. Banker GA, Cowan WM (1977) Rat hippocampal neurons in dispersed cell culture. *Brain Res* 126:397–425.
5. Groc L, et al. (2004) Differential activity-dependent regulation of the lateral mobilities of AMPA and NMDA receptors. *Nat Neurosci* 7:695–696.
6. Tardin C, Cognet L, Bats C, Lounis B, Choquet D (2003) Direct imaging of lateral movements of AMPA receptors inside synapses. *EMBO J* 22:4656–4665.
7. Groc L, et al. (2006) NMDA receptor surface mobility depends on NR2A-2B subunits. *Proc Natl Acad Sci USA* 103:18769–18774.
8. Tovar KR, Westbrook GL (2002) Mobile NMDA receptors at hippocampal synapses. *Neuron* 34:255–264.
9. Zhao J, et al. (2008) Synaptic metaplasticity through NMDA receptor lateral diffusion. *J Neurosci* 28:3060–3070.
10. Yang J, Chamberlain SE, Woodhall GL, Jones RS (2008) Mobility of NMDA autoreceptors but not postsynaptic receptors at glutamate synapses in the rat entorhinal cortex. *J Physiol* 586:4905–4924.
11. Groc L, Gustafsson B, Hanse E (2002) Spontaneous unitary synaptic activity in CA1 pyramidal neurons during early postnatal development: Constant contribution of AMPA and NMDA receptors. *J Neurosci* 22:5552–5562.

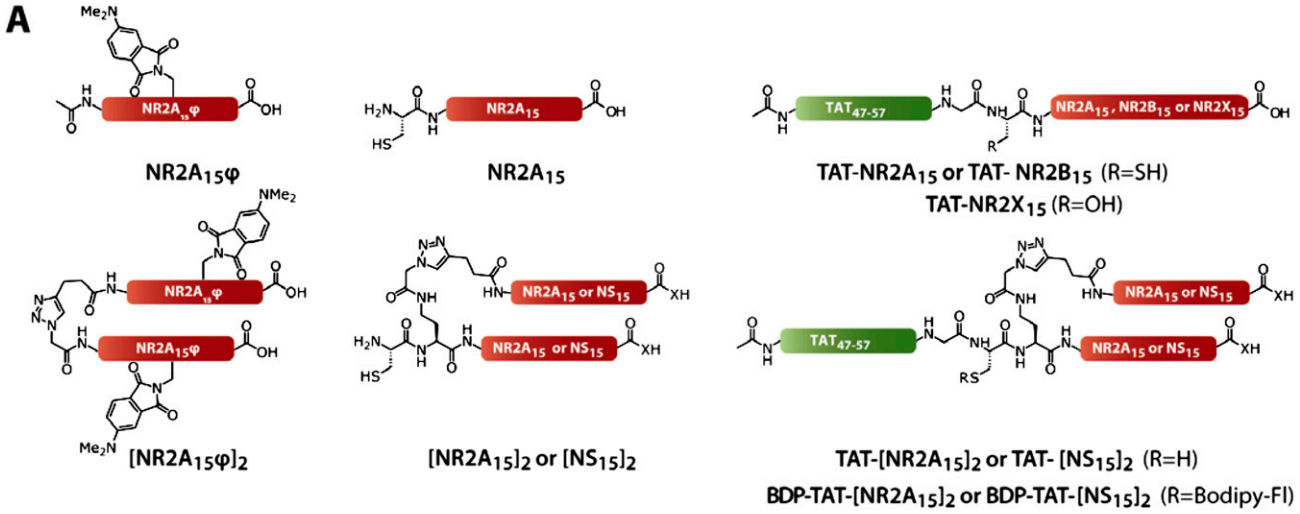

B

Name/Entry	Amino acid sequence
$NR2A_{15}$	-NRRVY KKλPS IESDV-COOH
$NR2A_{15}φ$	-NRRVY KKλPφ IESDV-COOH
$NR2B_{15}$	-NGHVY EKLSS IESDV-COOH
$NR2X_{15}$	-GGxxx xxxxS IESDV-COOH
NS_{15}	-YSLHA NTANR RTRPR-CONH2
TAT_{47-57}	-Y GRKKR RQRRR-
NR2A [rat, 1445-1464]	-LNSCS NRRVY KKMPS IESDV-COOH
NR2B [rat, 1463-1482]	-FNGSS NGHVY EKLSS IESDV-COOH
NR2C [rat, 1218-1237]	-TQGFP RSCTW RRVSS LESEV-COOH
NR2D [rat, 1304-1323]	-GGDLG TRRGS AHFSS LESEV-COOH
NR1 [rat, 919-938]	-RRAIE REEGQ LQLCS RHRES-COOH

C

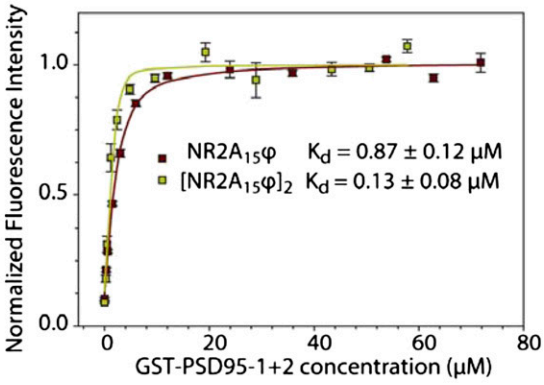

D

Ligand	t_R[a]	Formula (MH^+)	MH^+ calculated	MH^+ observed[b]
$NR2A_{15}φ$	25.9	$C_{92}H_{147}N_{26}O_{26}$	2033.3	2033.7
$[NR2A_{15}φ]_2$	30.5	$C_{187}H_{294}N_{55}O_{52}$	4144.7	4145.9
$NR2A_{15}$	24.3	$C_{82}H_{140}N_{25}O_{25}S$	1908.2	1908.2
$[NR2A_{15}]_2$	26.0	$C_{172}H_{287}N_{54}O_{52}S$	3975.6	3976.0
$[NS_{15}]_2$	23.0	$C_{164}H_{271}N_{70}O_{46}S$	3991.5	3991.3
TAT-$NR2A_{15}$	25.3	$C_{150}H_{261}N_{58}O_{40}S$	3549.1	3548.2
TAT-$NR2B_{15}$	26.0	$C_{143}H_{240}N_{53}O_{43}S$	3421.8	3422.9
TAT-$NR2X_{15}$	20.9	$C_{115}H_{203}N_{44}O_{38}$	2810.1	2811.0
TAT-$[NR2A_{15}]_2$	25.5	$C_{240}H_{408}N_{87}O_{67}S$	5616.5	5616.2
TAT-$[NS_{15}]_2$	27.9	$C_{232}H_{392}N_{103}O_{61}S$	5632.4	5631.2
BDP-TAT-$[NR2A_{15}]_2$	32.3	$C_{260}H_{429}BF_2N_{91}O_{70}S$	6030.7	6031.7
BDP-TAT-$[NS_{15}]_2$	38.6	$C_{252}H_{413}BF_2N_{107}O_{64}S$	6046.6	6047.0

Fig. S1. Structure and amino acid sequence of the competing ligands. (*A*) Structure of the monovalent and divalent ligands (X: O for $NR2A_{15}$ or NH for NS_{15}). (*B*) Sequences used for the peptide-based ligands of panel *A* and C-terminus residues of NMDAR subunits. φ, Dab(4-DMAP); λ, norleucine; x. . .x, PEG spacer (20 atoms; reference 01–63-0141; Novabiochem). Critical residues at positions 0 and −2 are highlighted (green for the common residues found in PSD-95 ligands, red otherwise). (*C*) Fluorescence titrations of the 4-DMAP-containing ligands with recombinant GST-PSD95-1+2. (*D*) Peptide-based ligands characterization. Purity was assessed by analytical reverse-phase HPLC (YMC C18, ODS-A 5/120, 250 × 4.6 mm) using a standard gradient (5% acetonitrile containing 0.1% TFA for 5 min followed by 5–95% acetonitrile containing 0.1% TFA over 50 min in water containing 0.1% TFA at a flow rate of 1 mL min^{-1}). All peptide-based ligands were more than 95% pure as judged by analytical HPLC. [[a]t_R indicates retention time; [b]peptide-based ligands identity was confirmed by MALDI-TOF MS (Voyager; PerSeptive Biosystems) using DHB as a matrix in linear or reflective modes.]

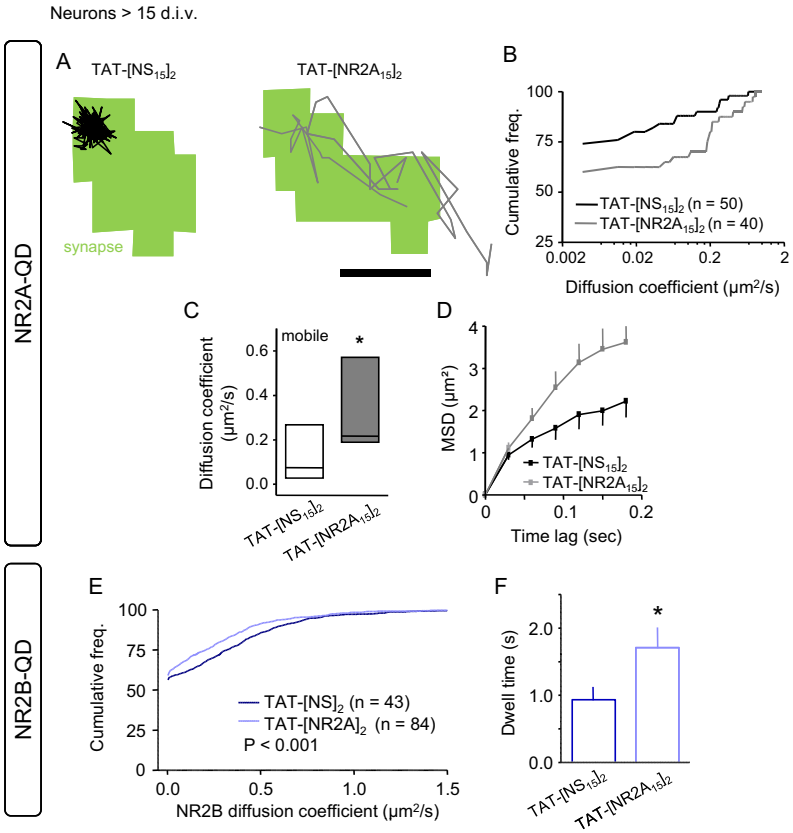

Fig. S2. TAT-[NR2A$_{15}$]$_2$ increases the mobility of synaptic 2A-NMDARs and decreases the mobility of 2B-NMDARs in mature (>15 d in vitro) synapses. (*A*) Representative trajectories of synaptic QDs coupled to NR2A after 10 to 20 min of incubation with TAT-[NS$_{15}$]$_2$ (*Right*) or TAT-[NR2A$_{15}$]$_2$ (*Left*). The gray regions correspond to synaptic sites labeled with Mitotracker. (Scale bar: 500 nm.) (*B*) Distribution of the diffusion coefficients of synaptic trajectories (bin size, 0.0075 μm^2/s). The first point of the curve corresponding to the proportion of immobile receptors shows the increase in mobility of 2A-NMDARs following incubation with TAT-[NR2A$_{15}$]$_2$. (*C*) The diffusion coefficient of mobile synaptic receptors is significantly increased in the presence of TAT-[NR2A$_{15}$]$_2$ (n = 13 trajectories/group; *$P < 0.05$, Mann–Whitney test). (*D*) Plot of the MSD (in μm^2) versus time lag (in s) for synaptic 2A-NMDARs in presence of TAT-[NS$_{15}$]$_2$ or TAT-[NR2A$_{15}$]$_2$. (*E*) Distribution of the diffusion coefficients of NR2B synaptic trajectories. Note the significant shift toward lower values. (*F*) The synaptic 2B-NMDAR dwell time was significantly increased in presence of TAT-[NR2A$_{15}$]$_2$.

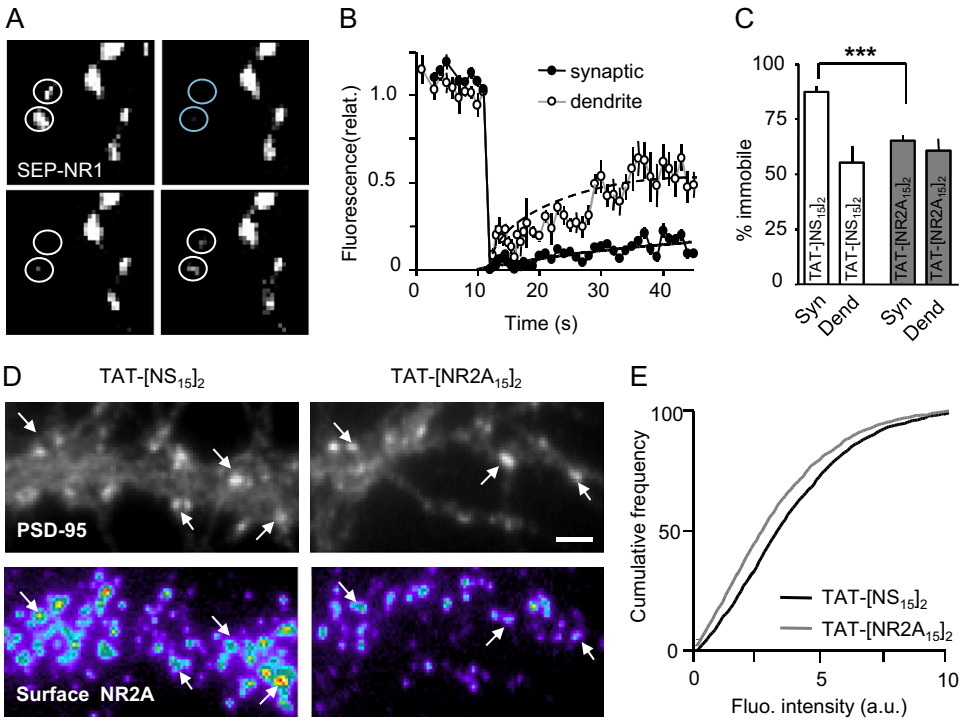

Fig. S3. Acute disruption of the interaction between 2A-NMDARs and PDZ proteins increases the surface diffusion of surface NR1-NMDARs and decreases the synaptic content of NR2A subunits. (*A* and *B*) Clusters of SEP-NR1 were photobleached and the recovery of the fluorescence was followed over a period of 50 s and expressed as recovery versus time on synaptic and dendrite areas. Note the higher proportion of immobile receptors within the synaptic compartment compared with the dendrite. (*C*) The average immobile fraction of synaptic and dendritic NMDARs are quantified after incubation with TAT-$[NS_{15}]_2$ (n = 52 synaptic clusters; n = 21 dendritic clusters) or TAT-$[NR2A_{15}]_2$ (n = 61 synaptic clusters; n = 20 dendritic clusters). Note the specific decrease of the proportion of immobile receptors within the synaptic area compared with the dendrite (***$P < 0.001$, t test). (*D*) Immunostaining of PSD-95 (synapse) and surface NR2A subunits in the presence of TAT-$[NR2A_{15}]_2$ or TAT-$[NS_{15}]_2$. Arrowheads represent synapses, i.e., PSD-95 cluster. (Scale bar: 5 μm.) (*E*) Fluorescence intensity of surface NR2A subunits in synapses (TAT-$[NR2A_{15}]_2$, n = 1,684 synapses; TAT-$[NS_{15}]_2$, n = 1,981).

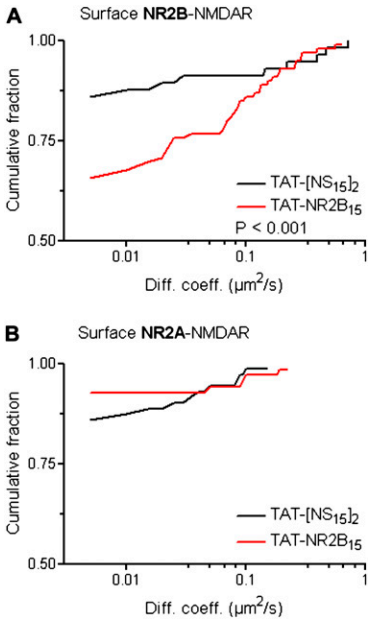

Fig. S4. TAT-$NR2B_{15}$ ligand specifically alters the surface diffusion of 2B-NMDARs without affecting the one of 2A-NMDARs. (*A*) Distribution of the diffusion coefficients of synaptic surface NR2B-NMDARs in presence of the nonsense or TAT-$NR2B_{15}$ ligand (5 μM, 10–15 min). Note the significant shift of the distributions in presence of TAT-$NR2B_{15}$, consistent with an increase diffusion (nonsense, n = 57; TAT-$NR2B_{15}$, n = 99 trajectories; $P < 0.001$). (*B*) Distribution of the diffusion coefficients of synaptic surface NR2A-NMDARs in presence of the nonsense or TAT-$NR2B_{15}$ ligand (5 μM, 10–15 min). No significant effect was observed (nonsense, n = 71; TAT-$NR2B_{15}$, n = 68 trajectories; $P > 0.05$).

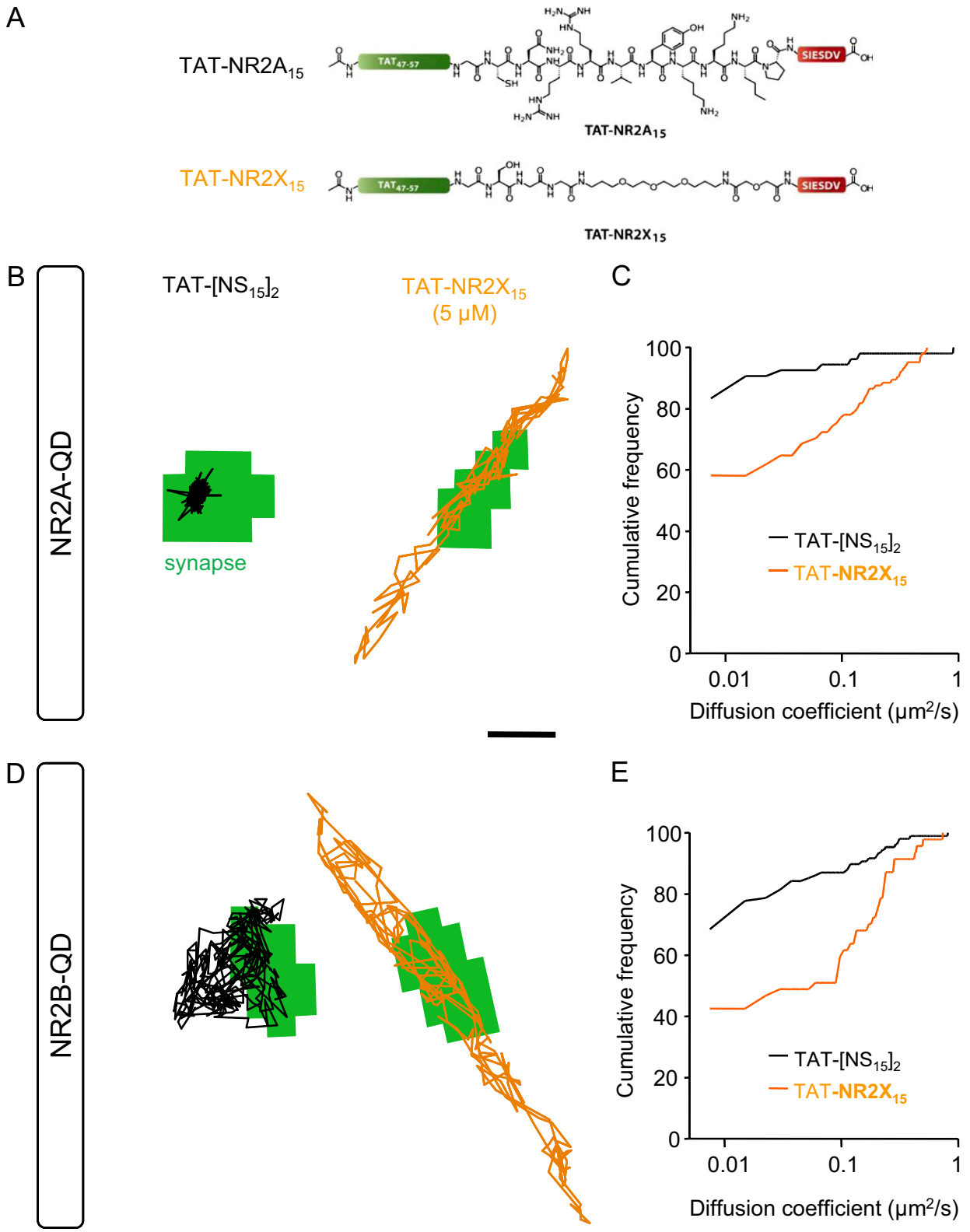

Fig. S5. TAT-NR2X$_{15}$ increases in a nonspecific manner the mobility of synaptic 2A- and 2B-NMDARs. (*A*) Comparison of TAT-NR2X$_{15}$ and TAT-NR2A$_{15}$ ligands. The TAT-NR2X$_{15}$ ligand comprises the last six residues of the C terminus of both NR2A and NR2B subunits (–SIESDV), a linker composed of PEG and glycine residues that provides a neutral backbone preventing any specific amino acid side chain interactions while maintaining the TAT sequence at a similar distance to that used for the other NR2A- and NR2B-derived ligands. (*B*) Representative trajectories of synaptic QDs coupled to NR2A after 10 to 20 min of incubation with TAT-[NS$_{15}$]$_2$ (*Left*) or TAT-NR2X$_{15}$ (*Right*). The green regions correspond to synaptic sites labeled with Mitotracker. (Scale bar: 500 nm.) (*C*) Cumulative distribution of the diffusion coefficients of synaptic trajectories (bin size, 0.0075 μm^2/s). The first point of the curve corresponds to the proportion of immobile receptors. Note the significant increase mobility of 2A-NMDARs following incubation with TAT-NR2X$_{15}$ ligand (TAT-[NS$_{15}$]$_2$, n = 54; TAT-NR2X$_{15}$, n = 105 trajectories; $P < 0.001$). (*D*) Representative trajectories of synaptic QDs coupled to NR2B after 10 to 20 min of incubation with TAT-[NS$_{15}$]$_2$ (*Left*) or TAT-NR2X$_{15}$

Legend continued on following page

(*Right*). The green regions correspond to synaptic sites labeled with Mitotracker. (Scale bar: 500 nm.) (*E*) Cumulative distribution of the diffusion coefficients of synaptic trajectories (bin size, 0.0075 $\mu m^2/s$). The first point of the curve corresponds to the proportion of immobile receptors. Note the significant increase mobility of 2B-NMDARs following incubation with TAT-NR2X$_{15}$ ligand (TAT-[NS$_{15}$]$_2$, n = 108; TAT-NR2X$_{15}$, n = 47 trajectories; $P < 0.01$).

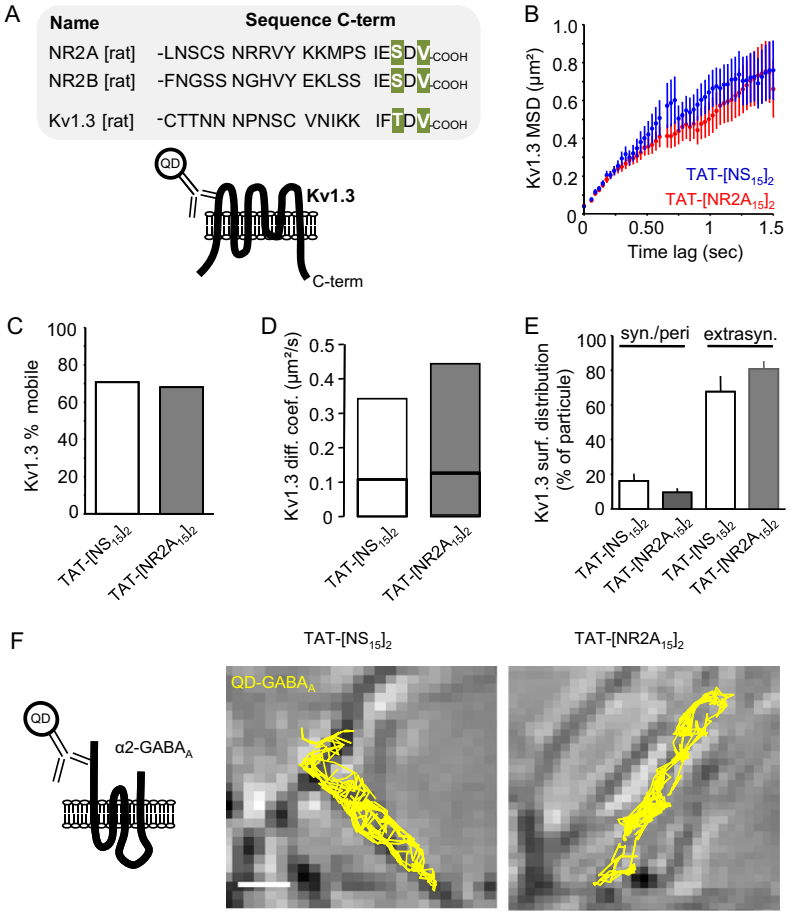

Fig. S6. Impact of TAT-[NR2A$_{15}$]$_2$ on potassium Kv1.3 channel and GABA$_A$ receptor surface trafficking. (*A*) Amino acid sequences of NR2A, NR2B, and Kv1.3 C-termini (*Rattus norvegicus*). Note the high similarity among the three sequences in the last 5 aa, in the known PDZ binding site. The tracking of endogenous Kv1.3 potassium channel was done by detecting an extracellular epitope of the channel using an antibody-QD complex (schematic representation, *Lower*). For the experiments below, we analyzed 116 trajectories in presence TAT-[NS$_{15}$]$_2$ and 209 trajectories in presence TAT-[NR2A$_{15}$]$_2$. (*B*) Plot of the MSD (in μm^2) versus time lag (in s) of surface Kv1.3 channel in presence of TAT-[NS$_{15}$]$_2$ or TAT-[NR2A$_{15}$]$_2$. No significant effect ($P > 0.05$). (*C*) The percent of mobile surface Kv1.3 channel remain statistically similar in presence of TAT-[NS$_{15}$]$_2$ or TAT-[NR2A$_{15}$]$_2$ ($P > 0.05$). (*D*) The distributions (median, 25–75% range) and medians of Kv diffusion coefficient were not significantly changed in presence of TAT-[NS$_{15}$]$_2$ or TAT-[NR2A$_{15}$]$_2$ ($P > 0.05$). (*E*) The surface distribution of Kv1.3 channels was examined using single particle live distribution. The Kv channels are mostly extrasynaptic (approximately 80%). Incubations with TAT-[NS$_{15}$]$_2$ (n = 6 dendritic fields) or TAT-[NR2A$_{15}$]$_2$ (n = 10 dendritic fields) did not affect the Kv1.3 channel surface distributions. (*F*) GABA$_A$ receptor surface diffusion was assessed using QDs coupled to an antibody directed against the α2 subunit of the receptor. Representative trajectories of single QDs show no effect on the mobility of GABA$_A$ receptors after 10 to 20 min of incubation with TAT-[NS$_{15}$]$_2$ or TAT-[NR2A$_{15}$]$_2$. (Scale bar: 1 μm.)

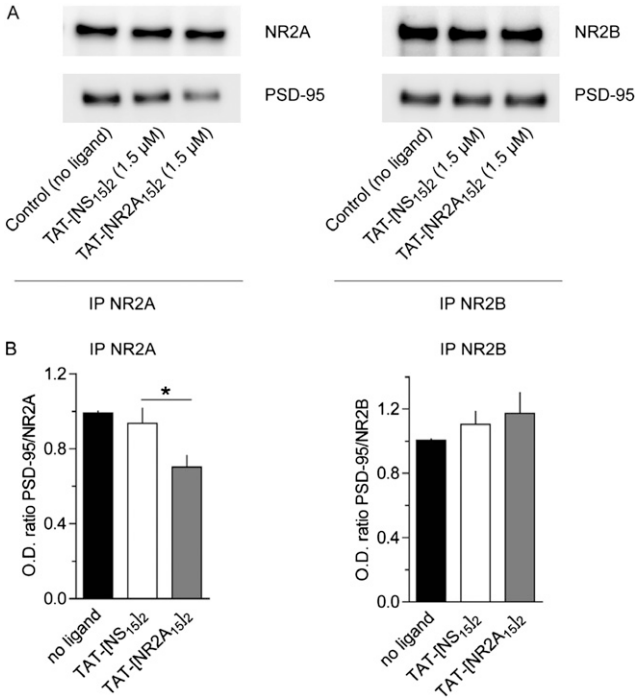

Fig. S7. TAT-[NR2A$_{15}$]$_2$ specifically blocks the interaction between PSD-95 and NR2A subunit in rat brain homogenates. (*A*) Representative gels of co-IP of PSD-95 with NR2 subunits in rat forebrain fractions treated with ligands. (*B*) TAT-[NR2A$_{15}$]$_2$ reduced the OD ratio of PSD-95:NR2A whereas induced no significant effect on OD ratio of PSD-95:NR2B. Values are means ± SEM (n = 5 for TAT-[NS$_{15}$]$_2$ and n = 8 for control and TAT-[NR2A$_{15}$]$_2$). Of note, although the specific effect of the divalent ligand could be monitored in brain lysates with solubilized protein complexes, we also observed for this approach a high sensitivity with respect to the nature of the detergents used in particular with the existence of a fine balance between conditions allowing for co-IP of the protein complexes of interest and conditions compatible with ligand-induced competition.

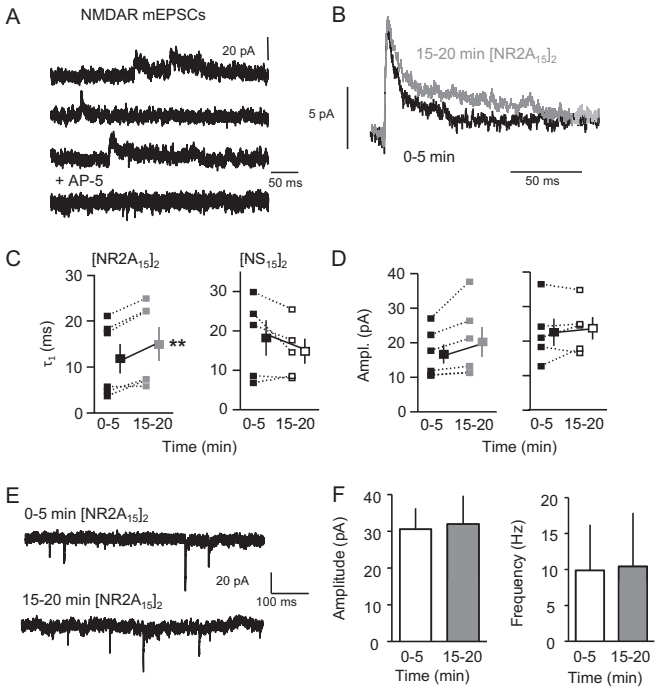

Fig. S8. The $[NR2A_{15}]_2$ functionally impacts only on miniature synaptic NMDAR currents. (*A*) Representative recordings of NMDAR mEPSCs at +30mV in the presence of Ca^{2+}/Mg^{2+} (2/2 mM), NBQX (10 μM; AMPAR antagonist), and bicuculline (20 μM; $GABA_A$ antagonist) in the whole cell configuration. The addition of AP-5 (25 μM) into the bath solution rapidly abolished NMDAR mEPSCs (*Lower*). The NMDAR mEPSC frequency range between 0.2 and 0.9 Hz, indicating that, on average, one event was detected every 2 s and overlap between events (example, *Upper*) was rare. (*B*) Averaged traces of NMDAR mEPSCs for two different time intervals: 0 to 5 min (black) and 15 to 20 min (gray) in the presence of $[NR2A_{15}]_2$ (5 μM) in the pipette solution. Note the slower decay after 15 to 20 min infusion compared with 0 to 5 min. (*C*) Time constants, τ_1, of the two time intervals (0–5 and 15–20 min). The decay was fitted using an exponential fit with a fast τ_1 and a slower τ_2 components. In the presence of $[NR2A_{15}]_2$ ($n = 6$ neurons) τ_1 was significantly increased (**$P < 0.01$, paired *t* test) whereas no effect was observed in the presence of $[NS_{15}]_2$ ($n = 5$ neurons; $P > 0.05$, paired *t* test). The same results were obtained with the slower τ_2 component. (*D*) Amplitude of NMDAR mEPSCs for the two time intervals (0–5 and 15–20 min) in the presence of $[NR2A_{15}]_2$ or $[NS_{15}]_2$ ($P > 0.05$, paired *t* test). (*E*) Representative traces of AMPAR mEPSCs recorded at −50 mV and isolated with 1 μM TTX, 20 μM bicuculline, and 25 μM AP5 during two time intervals: 0 to 5 min (*Upper*) and 15 to 20 min (*Lower*) after whole cell configuration. (*F*) Neither the amplitude nor the frequency of AMPAR mEPSCs was affected by $[NR2A_{15}]_2$ ($n = 6$ neurons).

A

Subunit	$NR2A_{15}$		$NR2B_{15}$	$NR2X_{15}$
	Monovalent	Divalent	Monovalent	Monovalent
NR2A	+	+++	-	+
NR2B	-	-	+	+
NR2A-S1462A		-		
$GABA_A$		-		
Kv1.3		-		

(-) No detectable change in diff. (+) Higher diffusion (+++) Very high diffusion

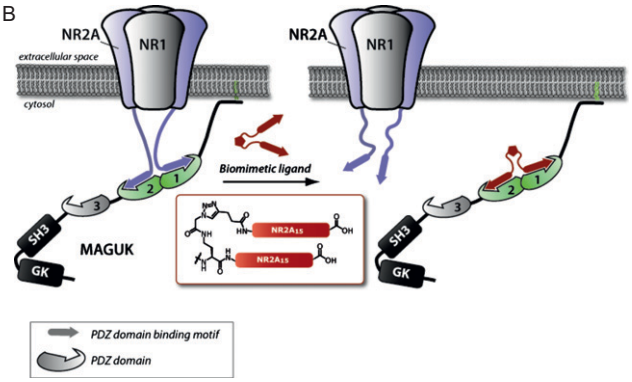

Fig. S9. Working model of TAT-$[NR2A_{15}]_2$. (*A*) Summary table of the impact of NR2-derived ligands on the synaptic diffusion of various surface subunits. (*B*) In basal conditions, 2A-NMDARs interact with MAGUK proteins like PSD-95 through their C-terminal PDZ binding domain. This interaction strongly retains 2A-NMDARs within the synapse. The divalent ligand (TAT-)$[NR2A_{15}]_2$ containing two binding motifs competes with 2A-NMDARs for the binding to specific interactors. This highly specific competition induces a destabilization of 2A-NMDARs.

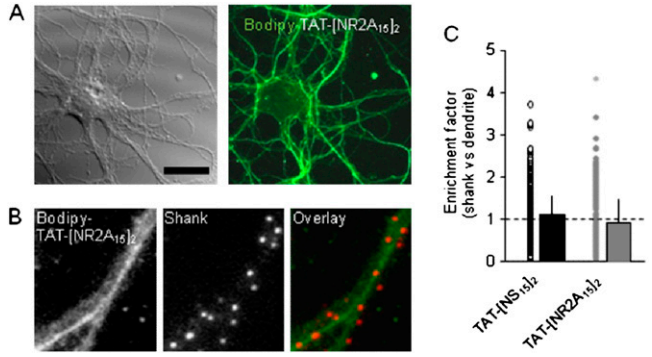

Fig. S10. Transduction of the BODIPY-TAT-$[NR2A_{15}]_2$ ligand in hippocampal cultured neurons. (*A*) Neurons were incubated for 5 min with 50 μM pyrene butyrate and for 10 min with 5 μM Bodipy-TAT-$[NR2A_{15}]_2$. Note the high transduction efficiency of the ligand within almost all processes. (Scale bar: 10 μm.) (*B*) Colocalization of TAT-$[NR2A_{15}]_2$ ligand with the postsynaptic marker shank. Neurons were incubated with 50 μM pyrene butyrate followed by 10 min with 5 μM TAT-$[NR2A_{15}]_2$. After a 20-min wash, cells were fixed in PFA 4%/sucrose 4% in PBS solution for 15 min. They were then permeabilized using Triton 0.1% in PBS solution. Neurons were incubated for 30 min with a rabbit anti-shank 3 antibody and for 30 min with a secondary anti-rabbit antibody coupled to an Alexa 568. (*C*) Consistent with the use of a saturating ligand concentration, no significant synaptic enrichment of both ligands was observed (TAT-$[NS_{15}]_2$, n = 939 synapses; TAT-$[NR2A_{15}]_2$, n = 426 synapses).

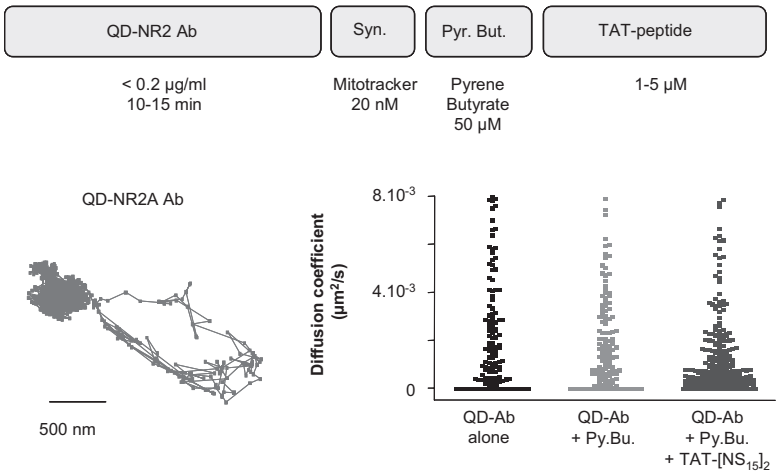

Fig. S11. Effect of pyrene butyrate and TAT peptide on basal NR-NMDAR surface diffusion. The nonspecific effects of pyrene butyrate or TAT-$[NS_{15}]_2$ was tested on the mobility of 2A-NMDARs. Whereas pyrene butyrate had no effect per se, TAT-$[NS_{15}]_2$ increased the proportion of immobile receptors. Such effect of TAT-$[NS_{15}]_2$ was observed on 2B-NMDARs, GluR2-AMPARs, $GABA_A$Rs, and reproduce using the monomeric TAT-$[NS_{15}]$. This indicates that TAT-NS slightly reduced the surface trafficking of neurotransmitter receptors, irrespective of the nature of the receptors or the structure of the TAT ligand.